Original Article

Institution of MECHANICAL ENGINEERS
Journal of AEROSPACE ENGINEERING

Proc IMechE Part G:
J Aerospace Engineering
0(0) 1–13

DOI: 10.1177/0954410019883097
journals.sagepub.com/home/pig
SAGE

Effect of propeller-induced flow on the performance of biplane micro air vehicle dynamics

Shuvrangshu Jana, Harikumar Kandath, Mayur Shewale and M Seetharama Bhat

Abstract

This paper presents the analysis of propeller-induced flow effects on the dynamics of a fixed wing biplane micro air vehicle. The analysis is based on wind tunnel tests and mathematical modeling. This analysis plays a pivotal role because the propeller-induced flow has significant effects on the dynamics of fixed wing micro air vehicle due to submergence of a large portion of the wing in propeller slipstream. Although the effect of the propeller-induced flow on the various aerodynamic parameter is reported in the literature; however, its effects on overall forces, moments and vehicle dynamics are not quantified so far. In this paper, propeller-induced flow effects are modeled as a function of motor rotation speed and mathematical analysis is performed to quantify their effects. The wind tunnel test is conducted at different propeller speeds on a biplane micro air vehicle "Skylark", having wingspan and chord length of 150 mm and 140 mm, respectively. Analysis of results shows that the propeller slipstream increases the overall lift, drag, side force, range, and endurance significantly. Propeller flow also contributes to the rolling moment and the pitching moment, while it has negligible effects on the yawing moment. It is shown that the trim angle of attack is lower when the propeller flow is considered in computing the trim conditions.

Keywords

Propeller-induced flow, micro air vehicle, modeling, biplane, fixed wing

Date received: 25 October 2018; accepted: 9 September 2019

Introduction

Micro air vehicles (MAVs) are soon becoming one of the essential assets in search and rescue, reconnaissance, surveillance missions and are also gaining importance in a tactical environment.[1] Specifically, the vehicle whose maximum dimension is less than 150 mm and velocity around 10 m/s belongs to the class of MAVs.[2] Amongst the various types of MAVs, fixed wing MAVs are superior as they are silent, offer more endurance, can carry a higher payload, fly faster and higher, and are virtually undetectable.

Accurate modeling of vehicle dynamics is crucial for analyzing the stability and performance of the vehicle while performing a specific mission. As most of the wing is submerged in propeller slipstream, the propeller-induced flow has a significant contribution to the total forces and moments acting on the MAV.

The propeller-induced flow increases the kinetic energy of the free stream causing the flow of energy towards the downstream to be higher than the flow energy upstream of the propeller. The effect of propulsive force on the aerodynamics of wing for bigger size vehicles is reported in various open literature.[3–7] In general, the propeller-induced flow changes the lift curve slope, drag polar, and also affects the flow transition and flow separation due to the formation of a modified boundary layer; however, the effects of the propeller-induced flow to the overall aerodynamics of the vehicle is less for high aspect ratio wing and high Reynolds number flow.

MAVs are generally of low aspect ratio (AR) typically less than 2 and operated in low Reynolds number (typically 50,000–100,000). In this region, the lift to drag ($\frac{L}{D}$) ratio reduces drastically due to the formation of a laminar separation bubble.[8] The size of the propeller dimension to the wing

Micro Air Vehicle Laboratory, Department of Aerospace Engineering, Indian Institute of Science, Bengaluru, India

Corresponding author:
Shuvrangshu Jana, Micro Air Vehicle Laboratory, Department of Aerospace Engineering, Indian Institute of Science, Bengaluru 560012, Karnataka, India.
Email: shuvra.ce@gmail.com

dimension is comparable in the case of propeller-driven MAV; hence, the effect of the propeller-induced flow on the overall aerodynamics is quite significant as it influences the flow transition,[9] flow separation, flow reattachment and formation of laminar separation bubbles.[10] The important parameters that are affected by the propulsive forces are stall angle of attack (AoA),[11] lift coefficient (C_L), and drag coefficient (C_D),[12] the slope of lift versus AoA curve,[13] $\frac{L}{D}$ ratio,[14,15] pitching moment,[16] etc. Propeller flow also influences the transition from laminar flow to turbulent flow.[17] The aerodynamic performance and stability of the MAV strongly depend on the flow behavior generated from the propeller flow stream.

The behavior and characteristics of flow around an object can be investigated through simulation as well as from wind tunnel tests.[18–20] The effects of the propeller-induced flow on the aerodynamics of small scaled vehicle is performed through computational fluid dynamics (CFD) simulation[16,18,21–24] and also by conducting wind tunnel tests.[10,11,14,15,25–27] Wind tunnel test on MAV with a wingspan of 300 mm in Reynolds number range of 120,000–180,000 showed that the propeller-induced flow increases the lift coefficient at a higher AoA and delays the stall.[11] Similarly, experiments at Reynolds number 135,000 with motor rotation in the range of 8000–10,000 r/min with 300 mm wingspan model showed an increase of C_L at a higher AoA and increase of C_D with the propulsive flow.[12] The effects of propeller induced flow on C_L and C_D further increases with an increase in the speed of motor rotation. Similarly, the increase of lift, drag, and stall AoA with increasing slipstream to free stream velocity ratio is observed during wind test on a model with a wingspan of 252.0 mm and a chord length of 142.6 mm with a propeller diameter of 5.5 inches in the velocity range of 5–15 m/s.[25]

A significant delay in stall and increase in slope of the lift versus AoA is observed with the propeller-induced flow in the wind tunnel experiment on a flat plate with AR (2–4) at Reynolds number 60,000–90,000, and these quantities are found to increase with the increase in motor rotation rate.[13] In Chinwicharnam and Thipyopas,[10] wind tunnel test on a square planform wing having a span and chord length of 12 inches with a diameter of 8 inches in tractor configuration in the velocity range of 6–10 m/s and motor RPM of 6000–8000 also showed an increase in the slope of lift curve by 1–1.13 times due to prop-wash effects. In this case, the factor K of the induced drag is also reported to be 0.9–1.12 times due to propulsive flow.

In Deng et al.,[22] dual-time preconditioning and overset grid methodologies are employed to simulate the influence of propeller flow. The increment of the aerodynamic coefficient, stall AoA, and decrement of lift to drag ratio of MAV is observed due to propeller flow. In contrast, in the range of Reynolds number (30,000–80,000) and aspect ratio of the wing (2–5), the increment of $\frac{L}{D}$ ratio as high as 10–12 is reported due to increasing lift and reduction of pressure drag under the influence of propeller slipstream.[13] In another experiment, the decrease of $\frac{L}{D}$ ratio at a lower AoA and increase of $\frac{L}{D}$ ratio at a higher AoA due to the propeller slipstream is reported for the wind tunnel test on 9 inches wingspan model in the range of Reynolds number range of $5 \times 10^4 - 1 \times 10^5$. The configuration of the flow source also affects significantly the dynamics of flow.[28] Computational investigation of flow around Reynolds number 83,000 showed that tractor configuration increases the $\frac{L}{D}$ ratio slightly and pusher configuration decreases the $\frac{L}{D}$ ratio. Similarly, the increment of pitching moment[16] and slope of pitching moment curve[29] due to the propeller-induced flow is reported in Ahn and Lee.[16]

The vehicles used in the above-mentioned literature are monoplanes having a wingspan exceeding 150 mm. Although the effects of propulsive flow on the individual parameters are discussed in the above experiments, the effects on the overall system dynamics are not reported. In Harikumar et al.,[30] the nonlinear model of the "KH2013A" MAV having span and chord length within 150 mm is developed incorporating the propeller rotation; however, the propeller rotation is not separately modeled and its effects on the aerodynamic performance are not analyzed. In case of biplane configuration, the effect of propulsive flow due to different motor configurations on the aerodynamic efficiency of fixed wing biplane having AR equal to 1 and Reynolds number in the range of 55,250–110,500 is reported.[31] The propulsive configuration is found to be more efficient in terms of aerodynamic performance for the low-speed flight; however, specific effect of the propulsive-induced flow is not analyzed. As per the author's knowledge, the propeller slipstream effect on the aerodynamic parameters of fixed wing biplane is not reported so far in the open literature.

In this paper, the effects of the propeller-induced flow on the dynamics of a fixed-wing biplane MAV, called "Skylark", having a wingspan and chord length not exceeding 150 mm (AR = 1.07) is analyzed around Reynolds number of 67,000. Wind tunnel test of the biplane MAV "Skylark" is performed in free stream flow as well as with only propulsive flow at the different motor rotation rates in a tractor configuration. The mathematical model of the MAV is developed with and without propeller rotation to understand its effects on different aerodynamic parameters.

It is observed that the propeller-induced flow increases the lift force, drag force, side force and add negative rolling, pitching, and yawing moment to the overall system. The novelty of the paper lies in the following aspects:

- Mathematical quantification of the contribution of propeller rotation toward overall forces and moments from wind tunnel experimental data.

- Analysis of the propeller-induced flow for a fixed wing biplane MAV.

The rest of the paper is organized as follows. Details of the specification of the fixed wing biplane MAV used for wind tunnel testing is described in the "Vehicle parameters" section. In "Wind tunnel test" section, description of wind tunnel and test set up is discussed. The forces and moments acting on the vehicle due to the propeller-induced flow as well as free stream flow and their comparison are discussed in "Forces and moments" section. Section "Range and endurance" describes the effect of the propeller-induced flow on the range and endurance of the MAV. The relative contribution of force and moments due to the propeller rotation at a typical operating point of "Skylark" MAV are discussed in section "Trim point analysis".

Vehicle parameters

The summary of the parameters of "Skylark" MAV (shown in Figure 1) is given in Table 1.

The diameter of the propeller is 5 inches and the wingspan of MAV is 6 inches; clearly, most of the wing is affected by the propeller slipstream.

Velocity streamlines in case of propeller off condition at a nominal velocity of 8 m/s are shown in Figure 2. Different colours indicate velocity magnitude ranging from 0 to 11.9 m/s as shown in Figure 2. The magnitude of the velocity streamlines goes up to a maximum of 11.9 m/s near to the motor mount. The flow visualization is performed through CFD analysis.

Wind tunnel test

The wind tunnel test is performed in the Micro Air Vehicle Aerodynamics Research Tunnel (MART) at National Aerospace Laboratory (NAL) complex in India. The test is conducted in closed test sections in open circuit low-speed wind tunnel.

Tunnel description

The details of the wind tunnel geometry are given in Table 2. The schematic of wind tunnel is shown in Figure 3.

The mean flow velocity variation is observed in the range of −0.1–0.1%. The turbulence intensity level is observed to be within 0.1% for velocity up to 10 m/s and within 0.15% for the velocity range 10–45 m/s. The forces and moments are measured using Mini40, which is an ATI six-axis force and torque sensor that measures outputting forces and torques from all three Cartesian coordinates (x, y, z). At each time, an average of 5000 measurements is taken as the measured value. These forces and moments are transformed to lift force, drag force, side force, and moments along the body frame of "Skylark" for standard analysis. The possible range of important variables for the wind tunnel set up is mentioned in Table 3.

The uncertainties in the measured data are expressed as the sum of fixed uncertainty due to the precision of load cells and an uncertainty proportional to the measured variable, expressed in percentage. The total uncertainty is expressed for the measurement obtained for a velocity of 8 m/s in Table 4.

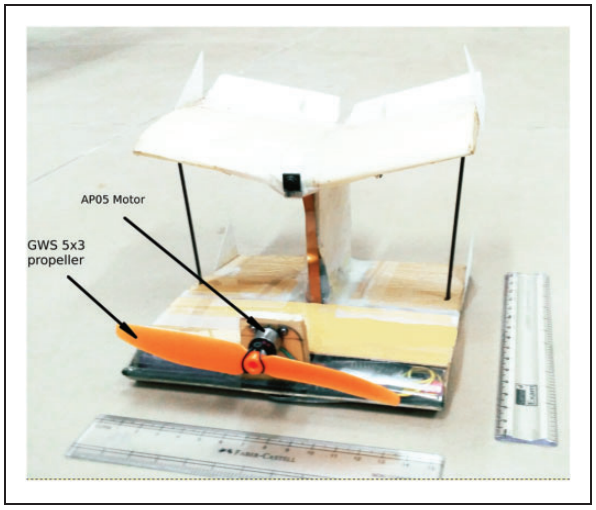

Figure 1. Photograph of "Skylark" MAV.

Table 1. "Skylark" specifications.

Component	Parameter	Value
Bottom wing	Span	150 mm
	Chord	140 mm
	Aerofoil	Modified MH-60
	Aerofoil thickness	12%
	Planform	Rectangular
Top wing	Span	150 mm
	Chord	85 mm
	Aerofoil	Modified MH-60
	Aerofoil thickness	8%
	Dihedral	12°
Vertical tail	Area	80 mm × 60 mm
	Height	80 mm
Control surface (Elevon)	Size (each)	75 mm × 26 mm
Winglet	Size (each)	45 mm × 30 mm
Motor	Type	Micro brushless
	Brand	AP05 5000 kV
Propeller	Brand	GWS 5030
	Diameter	5 inches
	Pitch	3 inches
Surface material	Wing	Balsa sheet
	Vertical tail	Depron
	Control surface	Depron

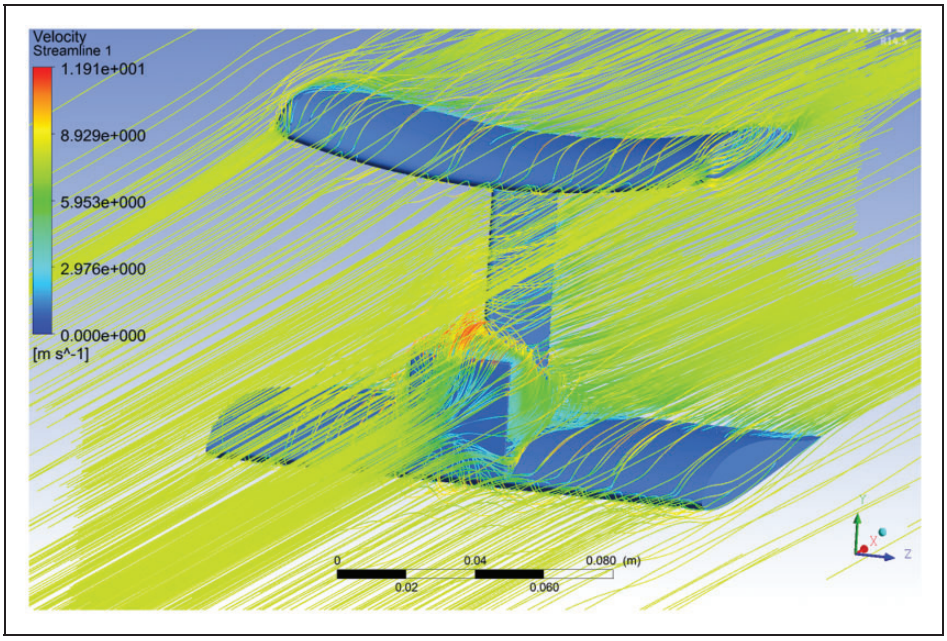

Figure 2. Velocity streamlines.

Table 2. Wind tunnel geometry.

Description	Specification
Test section	0.8 m × 1.2 m × 2.5 m
Contraction ratio	9:1
Tunnel length	17 m
Entry section	Bell shape with fitness ratio of 8
Type of honeycomb	Square cells
Turbulence screens	3 Nos.

Test set up

The test is performed in the velocity range of 6–16 m/s and for the full range of AoA and angle of sideslip. The flying model of " Skylark" is mounted inside the tunnel section, as shown in Figures 4 and 5.

The wind tunnel set up allows the automatic setting of the different position of the AoA, sideslip, and direct recording of the data from the balance sensor. Motor RPM is varied by varying the input throttle PWM. The test model is fitted with an autopilot with telemetry and a receiver. Throttle command is sent from a radio controller and received by the onboard receiver which then converts the command to an equivalent rotation speed command for the motor.

The input commands are transmitted to a ground station software using the telemetry port. The desired throttle PWM is maintained by observing the telemetry data at the ground station. The mapping between the motor RPM and the throttle PWM is developed beforehand using a tachometer. The similar technique is used to generate the control commands for varying the position of control surfaces.

Forces and moments

Details of the modeling of "Skylark" is discussed in literature.[32] In this paper, the forces and moments acting on the "Skylark" is discussed again for detailed analysis of the effect of the propeller-induced flow. In Figure 6, the different forces and moments acting on "Skylark" is shown as a schematic diagram.

The propeller-induced flow has significant effects on the lift force, drag force, and pitching moment, whereas side force, rolling moment, and the yawing moment is also affected due to the asymmetric flow distribution around the propeller. The side force and rolling moment due to propeller flow is quite significant if vertical surfaces like a vertical tail are placed in the propeller wash. A significant part of the rolling moment is also contributed from motor counter-torque. Combined effects of the propeller-induced flow and motor counter-torque on different forces and moments are modeled as a function of motor RPM.

Forces and moments are modeled separately due to free stream flow and due to the combined effect of the propeller-induced flow and motor counter-torque. The static derivatives and control derivatives are measured using the wind tunnel test while the dynamic derivatives are measured using standard empirical results.[33] It is to be noted that during wind tunnel test all the forces and moments are measured in vehicle body frame. Lift and drag forces are generally expressed in the stability frame; so, lift and drag forces are modeled in stability frame for ease in standard interpretation. For modeling purpose, the angles are expressed in radian and angular rates are expressed in rad/s.

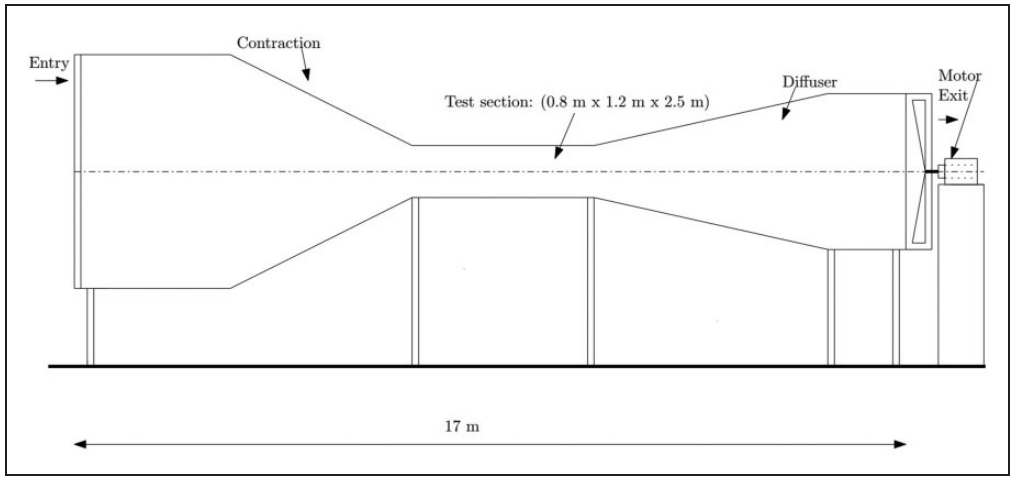

Figure 3. Schematic of wind tunnel used for testing the MAV.

Table 3. Possible test condition.

Description	Specification
Velocity range	1–45 m/s
Angle of attack	-4° to 32°
Angle of sideslip	-7° to 7°

Table 4. Uncertainties at velocity of 8 m/s.

Quantity	Uncertainties
Lift force	1.0 g + 6%
Drag force	0.5 g + 6%
Rolling moment	1.25 g-cm + 6%
Pitching moment	1.25 g-cm + 6%
Yawing moment	1.25 g-cm + 6%

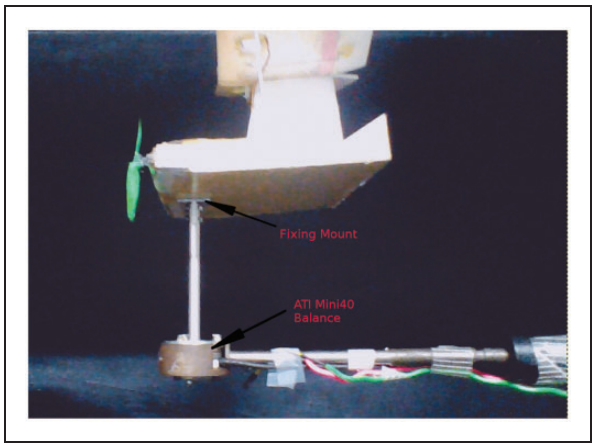

Figure 4. Mounting of MAV in wind tunnel.

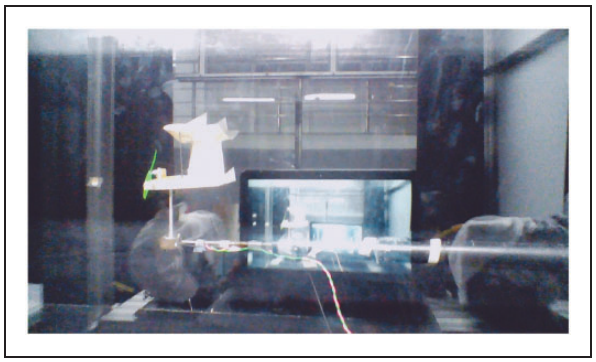

Figure 5. Snapshot of MAV in wind tunnel.

Lift and drag force

Lift and drag forces acting on MAV at any instant mainly depend on the elevator deflection (δ_e), vehicle AoA (α), pitch rate (q), and motor RPM (ω). Lift and drag forces are expressed in equations (2) to (6)

$$F_{Lift} = \frac{1}{2}\rho V_a^2 S\left(C_L(\alpha) + C_{L_q}\frac{c}{2V_a}q + C_L(\delta_e)\right) + f_L(\omega) \tag{1}$$

$$F_{Drag} = \frac{1}{2}\rho V_a^2 S\left(C_D(\alpha) + C_{D_q}\frac{c}{2V_a}q + C_D(\delta_e)\right) + f_D(\omega) \tag{2}$$

$$C_L(\alpha) = -0.065 + 2.9\alpha - 2\alpha^2 \tag{3}$$

$$C_D(\alpha) = 0.15 + 0.1\alpha + 1.5\alpha^2 \tag{4}$$

$$f_L(\omega) = 0.0022 - 4.6\delta_\omega + 11\delta_\omega^2 - 5.8\delta_\omega^3 \tag{5}$$

$$f_D(\omega) = -0.003466 + 15.86\delta_\omega - 52.19\delta_\omega^2 + 57.52\delta_\omega^3 - 21.01\delta_\omega^4 \tag{6}$$

where, $\delta_\omega = \frac{\omega+9300}{22765}$.

In the above equations, $f_L(\omega)$, and $f_D(\omega)$ denotes the contribution of propeller flow to the lift and

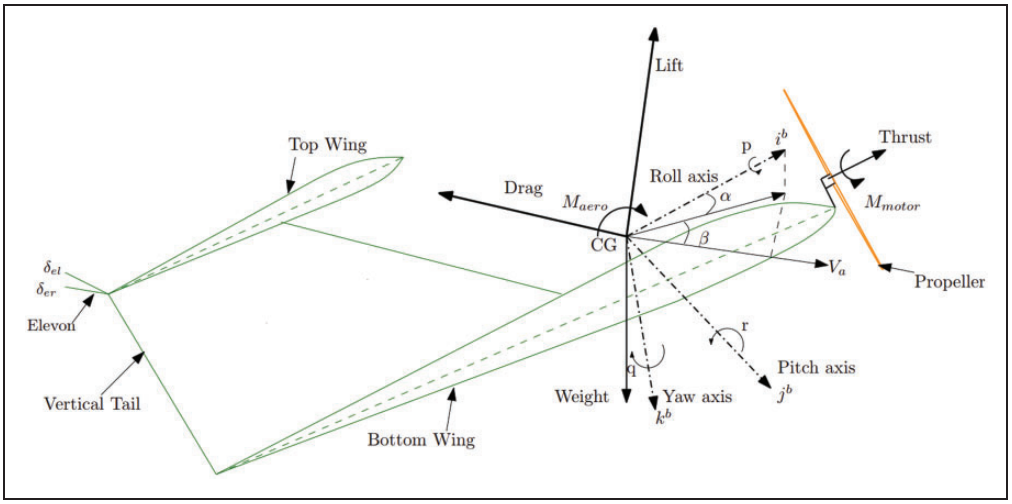

Figure 6. Diagram showing the axis convention, forces, and moments acting on MAV.

Table 5. Dynamic and control derivatives.

Dynamic	Value	Control	Value
C_{L_q}	1.1339	$C_L(\delta_e)$	$0.92\delta_e$
C_{D_q}	0	$C_D(\delta_e)$	$-0.06332\delta_e + 0.176\delta_e^2$

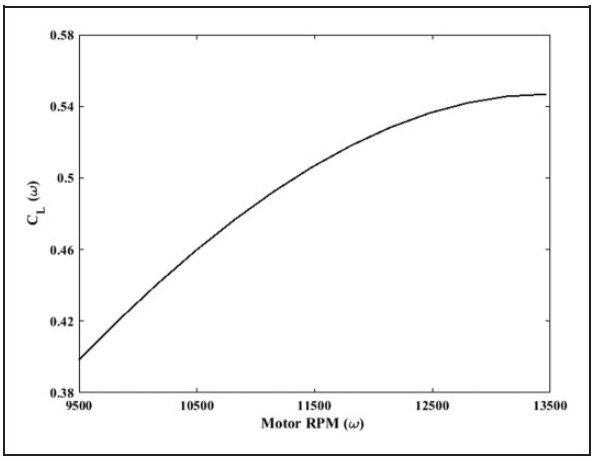

Figure 7. Lift coefficient vs motor RPM.

drag forces respectively. The expression for $f_L(\omega)$ and $f_D(\omega)$ are given in equations (5) and (6) respectively. The dynamic and control derivatives of the lift and drag force expression is mentioned in Table 5.

The variation of coefficient of lift only due to the propeller-induced flow as a function of motor RPM is shown in Figure 7, here $C_L(\omega) = f_L(\omega)/(0.5\rho V_a^2 S)$. Clearly, the lift force increases with the motor rotation as it imparts more kinetic energy to the flow.

The exact values of pitch rate, elevator angle, motor rotation corresponding to a particular AoA are difficult to set up in wind tunnel. Due to free stream flow, the amount of lift produced by the AoA of vehicle consist of a major portion of the total lift, as the effect of pitch rate and elevator angle is

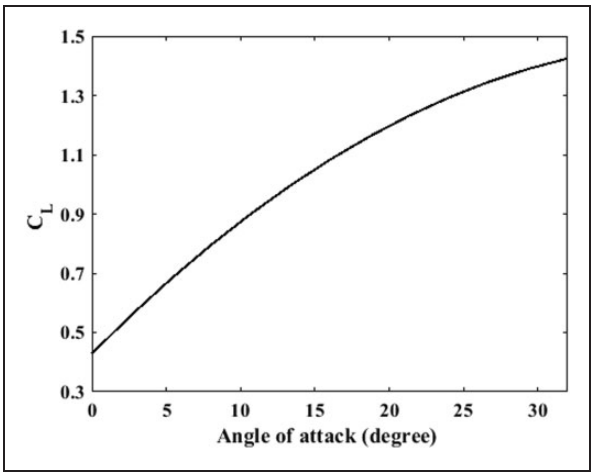

Figure 8. Total lift coefficient at 90 % throttle (motor RPM = 11,200).

comparatively low. For the analysis of the relative contribution of the propeller-induced flow towards the total lift, the effect of pitch rate and elevator angle is ignored. The exact contribution of the propeller-induced flow toward the total lift at a particular operating point is also analyzed at the end.

Figure 8 shows the variation of overall lift coefficient with AoA at the motor RPM of 11,200, here $C_L = F_{Lift}/(0.5\rho V_a^2 S)$. In Figure 8, the free stream flow is considered as 8 m/s and the RPM value is approximately 90% of the total throttle. At an AoA of 18° and free stream flow of 8 m/s, the lift force at a different percentage of the throttle is tabulated in Table 6. At 90% throttle, the lift force due to the propeller-induced flow is 54.40 g and the total lift is 125.81 g and, therefore, the propeller-induced flow increases the lift force by 76.18%. Clearly, in the case of small-scale vehicles lift force is strongly affected by the propeller-induced flow.

Similarly, for the analysis of drag force, the drag produced by the pitch rate and the elevator deflection

Table 6. Lift at different percentages of throttle.

Throttle	RPM	Lift due to propeller -induced flow (g)	Total lift (g)	% Increase of lift
85%	10,050	47.78	119.18	66.92
90%	11,200	54.40	125.81	76.18
95%	12,325	58.69	130.10	82.19
100%	13,465	60.22	131.63	84.33

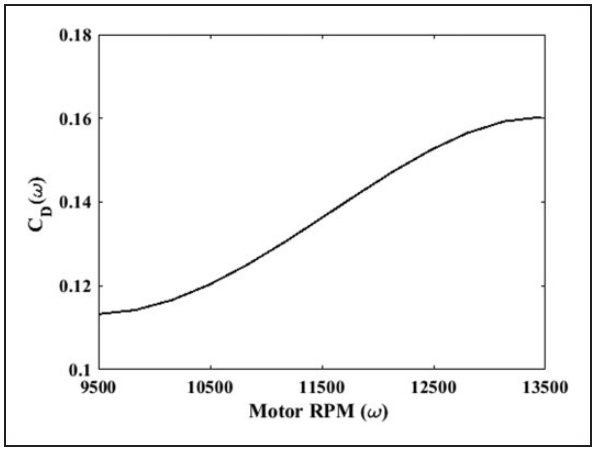

Figure 9. Drag coefficient vs motor RPM (ω).

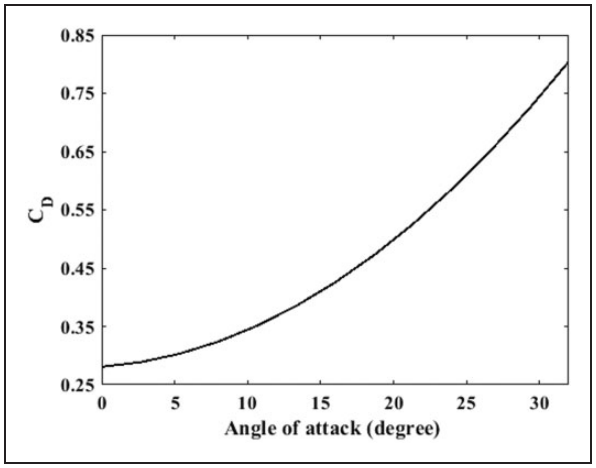

Figure 10. Total drag coefficient at 90% throttle (motor RPM = 11,200).

Table 7. Drag at different percentages of throttle.

Throttle	RPM	Drag due to propeller -induced flow (g)	Total drag (g)	% Increase of drag
85%	10,050	12.74	49.0	35.14
90%	11,200	14.40	50.67	39.70
95%	12,325	16.55	52.81	45.64
100%	13,465	17.65	53.92	48.66

is ignored. The variation of coefficient of drag only due to the propeller-induced flow is shown in Figure 9, $C_D(\omega) = f_D(\omega)/(0.5\rho V_a^2 S)$.

The total coefficient of drag due to the free stream flow of 8 m/s and the propeller-induced flow of 11,200 RPM is shown in Figure 10. At an AoA of 18°, the contribution of the propeller-induced flow towards total drag force at a different percentage of the throttle is shown in Table 7. The total drag force due to free stream flow of 8 m/s and propulsive flow of 11,200 RPM is 50.67 g, where propulsive flow contributed about 14.40 g. Clearly, the propulsive flow increases the drag by 39.70% at 90% throttle. Therefore, the propeller-induced flow has a significant effect on the total drag force.

Side force

The side force acting on the MAV mainly depends on the angle of sideslip (β), roll rate (p), yaw rate (r), aileron angle (δ_a), and asymmetric propeller flow. The side force is modeled in equations (7) and (8)

$$f_{Y_{aero}} = \frac{1}{2}\rho V_a^2 S\left(C_Y(\beta) + C_{Y_p}\frac{b}{2V_a}p + C_{Y_r}\frac{b}{2V_a}r + C_Y(\delta_a)\right) + f_Y(\omega) \tag{7}$$

$$f_Y(\omega) = 6.658 \times 10^{-7} - 0.4782\delta_\omega + 1.188\delta_\omega^2 - 0.639\delta_\omega^3 \tag{8}$$

where the dynamic and control derivatives terms are mentioned in Table 8.

The variation of side force coefficient with the motor rotation is shown in Figure 11, here $C_Y(\omega) = f_Y(\omega)/(0.5\rho V_a^2 S)$. The increment of side force with the increase of motor rotation is due to the asymmetric propeller-induced flow as well as the addition of more kinetic energy to the flow.

The contribution toward the side force with respect to the angle of sideslip and aileron angle is respectively plotted in Figures 12 and 13. Clearly from Figures 11 to 13, the relative magnitude of lateral force generated due to motor RPM is higher than sideslip angle and aileron angle. So, the propeller-induced flow is the major contributing factor toward the total side force acting on the system.

Rolling moment

The contributing factors behind the generation of the rolling moment (l) are the angle of sideslip, roll rate, pitch rate, aileron deflection, propeller-induced flow, and motor counter-torque. Due to the low moment of inertia of the fixed wing MAV, motor counter-torque

Table 8. Side force parameter.

Parameter	Value	Parameter	Value
$C_Y(\beta)$	$0.05 - 0.58\beta$	C_{Y_p}	0
C_{Y_r}	0	$C_Y(\delta_a)$	$0.1148\delta_a$

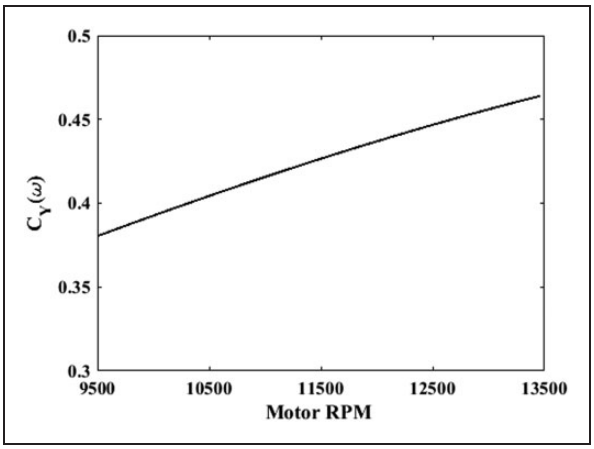

Figure 11. Side force coefficient vs motor RPM.

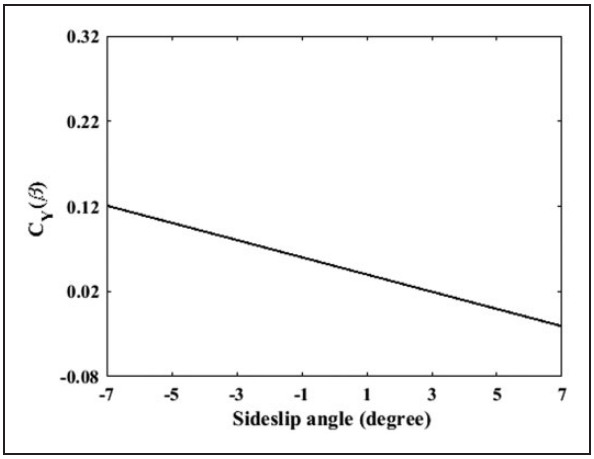

Figure 12. Contribution toward side force due to sideslip at zero aileron angle.

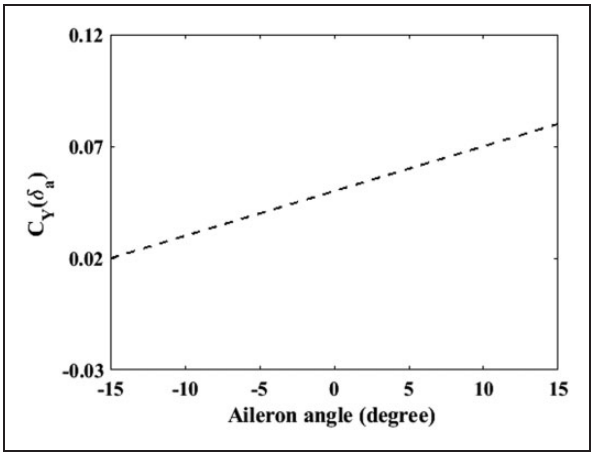

Figure 13. Contribution toward side force due to aileron at zero sideslip angle.

Table 9. Rolling moment coefficients.

Parameter	Value	Parameter	Value
$C_l(\delta_a)$	$-0.46\beta - 0.0059$	C_{l_p}	-0.0216
C_{l_r}	0.1639	$C_l(\delta_a)$	$0.14\delta_a$

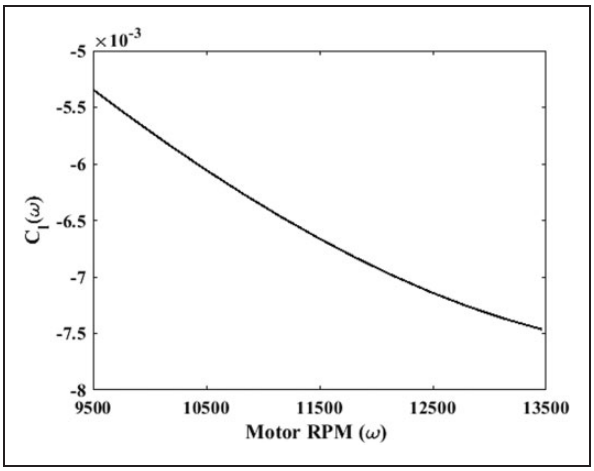

Figure 14. Rolling moment vs motor rotation.

contributes to a significant part of rolling moment acting on MAV. In equations (9) and (10), expression of rolling moment (l) is given

$$l = \frac{1}{2}\rho V_a^2 Sb\Big(C_l(\beta) + C_{l_p}\frac{b}{2V_a}p + C_{l_r}\frac{b}{2V_a}r + C_l(\delta_a)\Big) + f_l(\omega) \tag{9}$$

$$f_l(\omega) = 0.00041 + 0.05326\delta_\omega - 0.1351\delta_\omega^2 + 0.06991\delta_\omega^3 \tag{10}$$

where the rolling moment coefficients are expressed in Table 9.

The rolling moment coefficient generated due to the propeller-induced flow and motor counter-torque as a function of motor RPM is shown in Figure 14. In this case, the effect of counter-torque toward the generation of the rolling moment will have more contribution than the effect of propeller flow. The effect of counter-torque is very much specific to the selected combination of motor and propeller. Neglecting the effect of roll rate, yaw rate, and control surface deflection on the rolling moment, the variation of the total rolling moment coefficient as a function of the angle of sideslip at different motor rotations is shown in Figure 15. Similarly, at sideslip angle of 0°, the total rolling moment coefficient as a

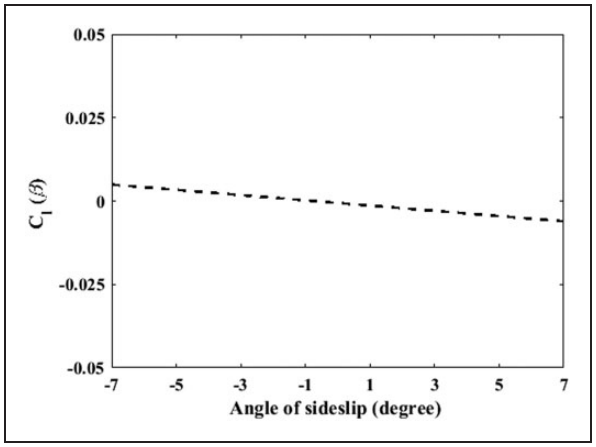

Figure 15. Contribution of sideslip angle toward rolling moment.

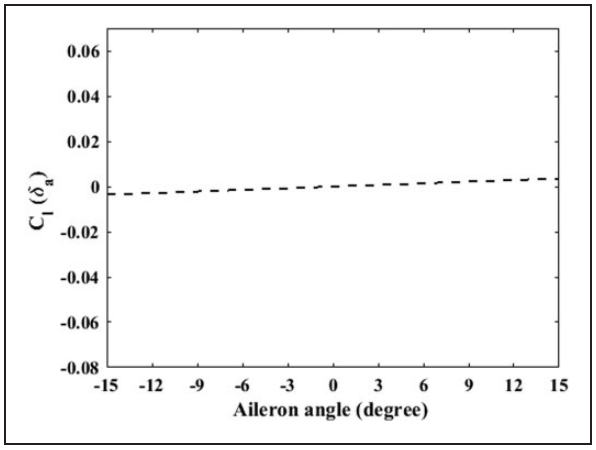

Figure 16. Contribution of aileron angle toward rolling moment.

function of aileron deflection at different motor rotations is plotted in Figure 16. For the purpose of comparison, considering no sideslip and aileron deflection of -5° the negative rolling moment due to the propeller-induced flow and motor counter-torque increases by 251% at 100% of throttle. It can be concluded that even after the selection of best motor-propeller combination, the moment contribution due to the propeller-induced flow and motor counter-torque is significant compared to aileron moment.

Pitching moment

Like lift and drag force, pitching moment (m) acting on the MAV depends on the AoA, pitch rate, elevator deflection, and motor rotation. The rotation of motor generates a pitching moment as a function of thrust and propeller-induced flow. In this vehicle, motor thrust axis passes through center of gravity; hence, the pitching moment due to motor rotation will be generated only due to the propeller-induced flow. The pitching moment is modeled

Table 10. Pitching moment coefficients.

Parameter	Value	Parameter	Value
$C_m(\alpha)$	$0.24 - 0.73\alpha$	$C_m(q)$	-0.2609
$C_m(\delta_e)$	$-0.5617\delta_e + 0.5703\delta_e^2$		

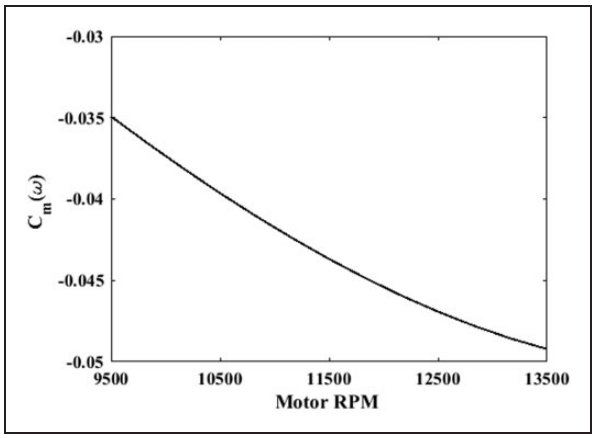

Figure 17. Pitching moment coefficient vs motor RPM.

in equations (11) and (12)

$$m = \frac{1}{2}\rho V_a^2 Sc\left(C_m(\alpha) + C_{m_q}\frac{c}{2V_a}q + C_m(\delta_e)\right) + f_m(\omega) \tag{11}$$

$$f_m(\omega) = -0.00019 + 0.33\delta_\omega - 0.8229\delta_\omega^2 + 0.4173\delta_\omega^3 \tag{12}$$

where the pitching moment coefficients are expressed in Table 10.

The variation of pitching moment coefficient as a function of motor rotation is shown in Figure 17. Figure 18 shows the total pitching moment as a function of the AoA at 90% throttle. Clearly, with an increase in the propeller-induced flow, the negative pitching moment becomes more negative. So, the propeller-induced flow reduces the value of the AoA at zero pitching moment as well as pitching moment at zero AoAs. The AoA corresponding to zero pitching moment and the pitching moment at zero AoA affects the plant aerodynamic performance as well as longitudinal stability.

Yawing moment

The main variables which affect the rolling moment are same as the yawing moment (n). Yawing moment is modeled in equations (13) and (14)

$$n = \frac{1}{2}\rho V_a^2 Sb\left(C_n(\beta) + C_{n_p}\frac{b}{2V_a}p + C_{n_r}\frac{b}{2V_a}r + C_n(\delta_a)\right) + f_n(\omega) \tag{13}$$

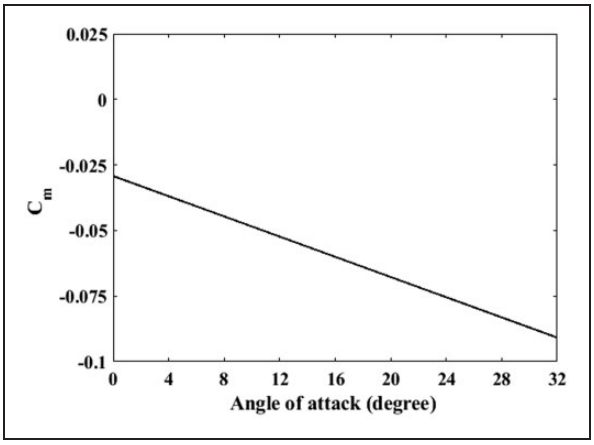

Figure 18. Pitching moment coefficient vs angle of attack.

Table 11. Yawing moment coefficients.

Parameter	Value	Parameter	Value
$C_n(\beta)$	$0.24\beta - 0.011$	C_{n_p}	0.0
C_{n_r}	–0.5375	$C_n(\delta_a)$	$0.09087\delta_a$

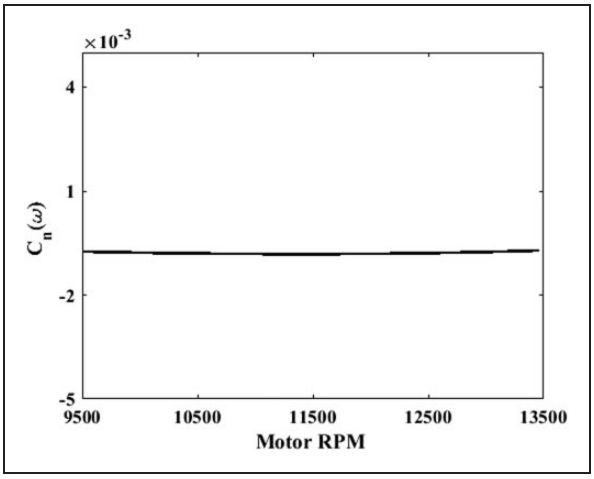

Figure 19. Yawing moment coefficient vs motor RPM.

$$f_n(\omega) = -0.0000997 + 0.01316\delta_\omega - 0.03349\delta_\omega^2 + 0.01925\delta_\omega^3 \tag{14}$$

where the yawing moment coefficients are expressed in Table 11.

The variation of the yawing moment coefficient with motor rotation is shown in Figure 19. The contribution of the sideslip angle toward the yawing moment coefficient is shown in Figure 20. Comparing the relative magnitude of the yawing moment from Figures 19 and 20 clearly, the propeller-induced flow does not have the significant effect on the overall yawing moment.

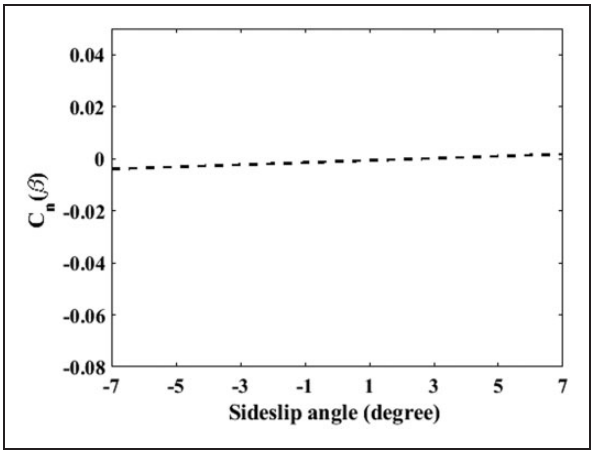

Figure 20. Contribution of sideslip angle toward yawing moment.

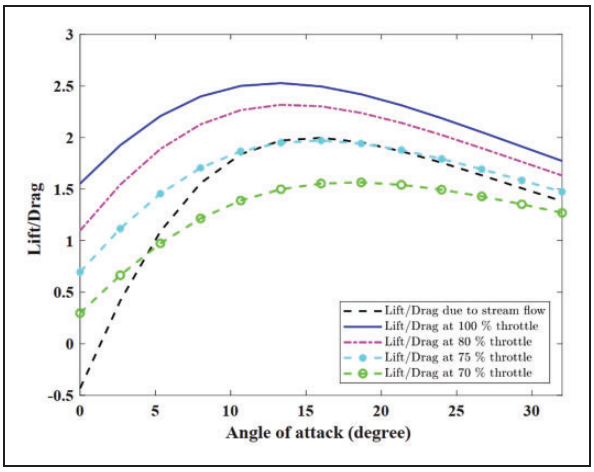

Figure 21. Contribution toward $\frac{\text{Lift}}{\text{Drag}}$ due to propeller-induced flow at different RPMs.

Range and endurance

The two important variables which affect the range and endurance of a vehicle are $\frac{C_L}{C_D}$ ratio and $\frac{C_L^{1.5}}{C_D}$ ratio. The range and endurance of a vehicle increases with the increase of these two parameters respectively. The $\frac{C_L}{C_D}$ ratio and $\frac{C_L^{1.5}}{C_D}$ ratio can be approximately correlated to $\frac{\text{Lift}}{\text{Drag}}$ ratio and $\frac{\text{Lift}^{1.5}}{\text{Drag}}$ ratio. The variation of $\frac{\text{Lift}}{\text{Drag}}$ as a function of AoA with different motor rotations is shown in Figure 21. In the case of 100% throttle (RPM = 13,465) and an AoA of 18°, the propulsive flow increases the $\frac{\text{Lift}}{\text{Drag}}$ ratio by 23.98%.

Figure 22 shows the variation of $\frac{\text{Lift}^{1.5}}{\text{Drag}}$ with AoA at different motor rotations. At 100% (RPM = 13,465) throttle and AoA of 18°, the propulsive flow increases the parameter $\frac{\text{Lift}^{1.5}}{\text{Drag}}$ by 68.26%. Clearly from Figures 21 and 22, the propeller-induced flow has a

positive effect on the range and endurance of the vehicle after a certain threshold of motor RPM.

Trim point analysis

The trim point analysis of the nonlinear model of the vehicle is performed with and without propulsive flow. The equilibrium value of the different states and control variables for steady and constant turning flight of radius 25 m, at the operating point for the nominal velocity of 8 m/s with and without propulsive flow, are tabulated in Table 12 with both the cases. The state variables are velocity (u, v, w), attitude (ϕ, θ, ψ), and attitude rates (p, q, r), whereas control variables are elevator (δ_e), aileron (δ_a), and throttle (δ_ω). The unit of velocity is in m/s, the attitude in degrees, attitude rate in degrees/s, and control variables are in degrees.

Comparing the trim values of the state variables in the case of the propeller-induced flow and with no propeller-induced flow clearly, trim values vary significantly due to the propeller-induced flow. The contribution of the propeller-induced flow to the overall forces and moments at the trim point are tabulated in Table 13.

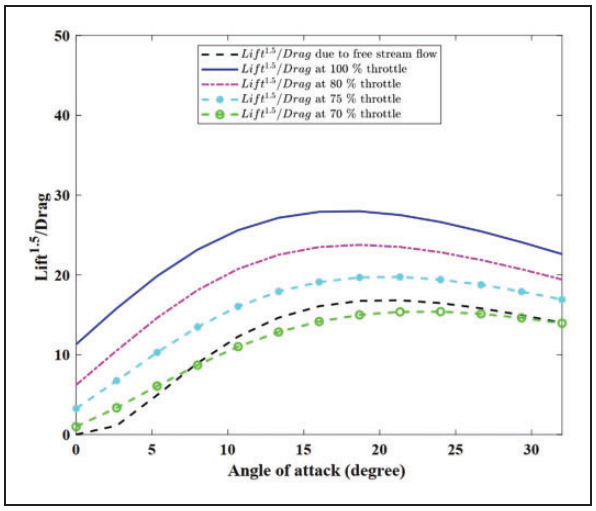

Figure 22. Contribution toward $\frac{\text{Lift}^{1.5}}{\text{Drag}}$ due to propeller-induced flow at different RPMs.

Table 12. Variation of trim point.

Variable	Without propeller-induced flow	With propeller-induced flow
u	7.34	7.66
v	0.11	−0.09
w	3.21	2.34
ϕ	−2.45	−5.56
θ	23.58	16.91
ψ	0	0
p	−0.37	−0.27
q	−0.03	−0.09
r	0.84	0.87
δ_e	−5.65	−13.64
δ_a	4.95	11.43
δ_ω	0.68	0.70

Results

Clearly, many of the aerodynamic parameters are significantly affected by the propeller flow. From Table 6 and 7, at RPM of 13,465 (100% throttle), lift coefficient and drag coefficient are respectively found to be increased by 84.33% and 48.66% due to the propulsive flow. At the same RPM of 13,465 and at an AoA of 18°, propulsive flow increases $\frac{C_L}{C_D}$ ratio and $\frac{C_L^{1.5}}{C_D}$ ratio by 23.98% and 68.26% respectively. Similarly, the combined effect of the propeller-induced flow and motor counter-torque increases the negative rolling moment by 251%. Propulsive flow affects the pitching moment by 40%, whereas the yawing moment remains unaffected. From Table 12, it is clear that there is also a significant variation of aerodynamic states due to propulsive flow. Specifically, it reduces the trim AoA but increases the trim roll angle.

Discussions

The effect of the propeller-induced flow on the MAV system dynamics is highly specific to the particular MAV configuration. However, a general conclusion can be drawn regarding the effect of the propeller-induced flow on MAV. The major points are as follows:

- Lift force: The amount of produced lift increases with the propulsive flow.

Table 13. Contribution of propeller flow at trim point.

Quantity	Total	Contribution due to propeller induced flow	% Contribution of propeller induced flow
Lift force (g)	61.64	17.87	28.99%
Drag force (g)	58.19	21.30	36.60%
Side force (N)	0.33	0.40	81.57%
Pitching moment (N-m)	0.0244	−0.0045	−18.34%

- Drag force: The total amount of drag produced by the combined effect of the propeller-induced flow and free stream flow is higher than the drag produced due to free stream flow, and it increases with motor RPM.
- Side force: Side force increases with the increase in the propulsive flow; however, its amount is highly dependent on the size of the vertical surface in the slipstream.
- Moments: The magnitude of the rolling moment and pitching moment increases with the propeller-induced flow. In case of rolling moment, motor counter-torque contributes to a major part of additional moment. Effect on yawing moment due to the propeller-induced flow is less.
- The range and endurance of the vehicle are significantly affected due to the propeller rotation, and after a threshold RPM, range and endurance of a vehicle increase with the propeller-induced flow.

Conclusions

Modeling and analysis of the propeller-induced flow on the dynamics of a fixed-wing biplane MAV are presented. The effect of propeller flow is modeled as a function of motor rotation from the wind tunnel test data. For a typical constant turning flight condition, the effect of propeller rotation approximately increased 28.99% of the lift force, 36.60% of the drag force, and 81.57% of the side force. Rolling and pitching are also being affected by a significant amount. The propeller-induced flow reduced the trim AoA and it further reduced with the increase of the rotation rate. Range and endurance increases with the propeller-induced flow. Clearly, the propeller rotation plays a crucial role in the aerodynamic performance and efficiency of MAV and its accurate modeling is important for the system design. The analysis in this paper will help in the design of MAV configuration.

Acknowledgements

The authors would like to thank National Aerospace Laboratory (NAL) for allowing them to conduct wind tunnel test. They would also like to thank Shashank Shivkumar, Susheel Balasubramaniam, Eshaan Khanapuri, Kuntal Ghosh for helping them in conducting wind tunnel test and flow simulation.

Declaration of Conflicting Interests

The author(s) declared no potential conflicts of interest with respect to the research, authorship, and/or publication of this article.

Funding

The author(s) disclosed receipt of the following financial support for the research, authorship, and/or publication of this article: The work was funded under National Programme for Micro Air Vehicle (NP-MICAV) project of Defence Research Development Organization (DRDO). The authors would like to thank Aeronautics Research and Development Board (ARDB) for their funding and support for the project.

ORCID iD

Shuvrangshu Jana https://orcid.org/0000-0001-8906-8519

References

1. Hassanalian M, Khaki H and Khosravi M. A new method for design of fixed wing micro air vehicle. *Proc I MechE, Part G: J Aerospace Engineering* 2015; 229: 837–850.
2. McMichael JM and Francis MS. Micro air vehicles-toward a new dimension in flight. *DARPA document* 1997.
3. Brenckmann ME. Experimental investigation of the aerodynamics of a wing in a slipstream. *J Aerosp Sci* 1958; 25: 324–328.
4. George M and Kisielowski E. Investigation of propeller slipstream effects on wing performance. Technical report, Dynasciences Corp Blue Bell PA, 1967.
5. Witkowski DP, Lee AK and Sullivan JP. Aerodynamic interaction between propellers and wings. *J Aircraft* 1989; 26: 829–836.
6. Catalano F. On the effects of an installed propeller slipstream on wing aerodynamic characteristics. *Acta Polytechnica* 2004; 44.
7. Veldhuis LLM. *Propeller wing aerodynamic interference*. PhD Thesis, Delft University of Technology, The Netherlands, 2005.
8. Shyy W, Lian Y, Tang J, et al. *Aerodynamics of low Reynolds number flyers,* volume 22. Cambridge: Cambridge University Press, 2007.
9. Aminaei H, Dehghan Manshadi M and Mostofizadeh AR. Experimental investigation of propeller slipstream effects on the wing aerodynamics and boundary layer treatment at low Reynolds number. *Proc I MechE, Part G: J Aerospace Engineering* 2018. DOI: 10.1177/0954410018793703.
10. Chinwicharnam K and Thipyopas C. Comparison of wing–propeller interaction in tractor and pusher configuration. *Int J Micro Air Veh* 2016; 8: 3–20.
11. Arivoli D, Dodamani R, Antony R, et al. Experimental studies on a propelled micro air vehicle. In: *Proceedings of the 29th AIAA applied aerodynamics conference,* Honolulu, Hawaii, vol. 3656, 27–30 June 2011.
12. Durai A. Experimental investigation of lift and drag characteristics of a typical MAV under propeller induced flow. *Int J Micro Air Veh* 2014; 6: 63–72.
13. Ananda GK, Deters RW and Selig MS. Propeller-induced flow effects on wings of varying aspect ratio at low Reynolds numbers. AIAA-2014-2152, 2014.
14. Ananda Krishnan GK, Deters RW and Selig MS. Propeller induced flow effects on wings at low Reynolds numbers. In: *31st AIAA applied aerodynamics conference*, 2013, p. 3193.
15. Null W, Noscek A and Shkarayev S. Effects of propulsive-induced flow on the aerodynamics of micro air vehicles. In: *23 rd AIAA applied aerodynamics conference*, Toronto, Canada, 6–9 June 2005, p.4616.

16. Ahn J and Lee D. Aerodynamic characteristics of a micro air vehicle and the influence of propeller location. In: *31st AIAA applied aerodynamics conference*, San Diego, CA, 24–27 June 2013, p.2655.
17. Ananda GK, Selig MS and Deters RW. Experiments of propeller-induced flow effects on a low-Reynolds-number wing. *AIAA J* 2018; 56: 3279–3294.
18. Choi S and Ahn J. A computational study on the aerodynamic influence of a pusher propeller on a MAV. In: *40th fluid dynamics conference and exhibit*, 2010, p. 4741.
19. Bakkhoshnevis A, Mamouri AR and Khodadadi S. Experimental investigation for wake of the circular cylinder by attaching different number of tripping wires. *Iran J Mech Eng Trans ISME* 2016; 17: 5–25.
20. Bakkhoshnevis A, Mamouri AR and Nazari M. Experimental investigation of wake on an elliptic cylinder in the presence of tripping wire. *Iran J Mech Eng Trans ISME* 2017; 18: 81–102.
21. Ageev N. Numerical investigation of disc-wing MAV with propeller in a wing slot. In: *International micro air vehicle conference and competitions*, t Harde, the Netherlands, 2011 (IMAV 2011), 2011.
22. Deng S, W van Oudheusden B, Xiao T, et al. A computational study on the aerodynamic influence of a propeller on an MAV by unstructured overset grid technique and low mach number preconditioning. *Open Aerosp Eng J* 2012; 5.
23. Khan W, Nahon M and Caverly R. Propeller slipstream model for small unmanned aerial vehicles. In: *AIAA modeling and simulation technologies (MST) conference*, Boston, MA, 19–22 August 2013, p.4907.
24. Sharpe P and Agarwal RK. Conceptual and numerical analysis of active wingtip vortex cancellation in propeller-driven electric aircraft. In: *AIAA Scitech 2019 Forum*, 2019, p. 1091.
25. Randall R, Hoffmann CA and Shkarayev S. Longitudinal aerodynamics of a vertical takeoff and landing micro air vehicle. *J Aircraft* 2011; 48: 166–176.
26. Sudhakar S, Kumar C, Arivoli D, et al. Experimental studies of propeller induced flow over a typical micro air vehicle. AIAA-2013-0060, 2013.
27. Sharma P and Atkins EM. An experimental investigation of tractor and pusher hexacopter performance. In: *2018 atmospheric flight mechanics conference*, Atlanta, USA, 25–29 June 2018, p.2983.
28. Khoshnevis AB, Barzenoni V and Mamouri AR. Experimental study of parameters and high-order values of velocity in the behind wake of a vehicle model. *Int J Autom Eng* 2016; 6: 2291–2300.
29. Spoerry MT and Wong K. Design and development of a micro air vehicle (μav) concept: Project bidule. In: *The 9th annual international aerospace congress*, University of Sydney, NSW, Australia, 2011.
30. Harikumar K, Dhall S and Bhat MS. Nonlinear modeling and control of coupled dynamics of a fixed wing micro air vehicle. In: *2016 Indian control conference (ICC)*, 2016, pp.318–323. New York: IEEE.
31. Thipyopas C and Moschetta J. A fixed-wing biplane MAV for low speed missions. *Int J Micro Air Veh* 2009; 1: 13–33.
32. Jana S. *Novel biplane micro air vehicle system with adaptive control and vision augmentation*. PhD Thesis, Indian Institute of Science, India, 2018.
33. Roskam J. *Airplane design*. vol. 6. Lawrence, KS: Roskam Aviation and Engineering Corporation, 1990.